


Absence of Evidence of Electrical Switching of the Antiferromagnetic Néel Vector

C. C. Chiang,¹ S. Y. Huang^{1,*}, D. Qu,² P. H. Wu,¹ and C. L. Chien^{1,2,3}¹*Department of Physics, National Taiwan University, Taipei 10617, Taiwan*²*Institute of Physics, Academia Sinica, Taipei, 11529, Taiwan*³*Department of Physics and Astronomy, Johns Hopkins University, Baltimore, Maryland 21218, USA* (Received 23 July 2019; revised manuscript received 16 September 2019; published 27 November 2019)

Much theoretical and experimental attention has been focused on the electrical switching of the antiferromagnetic (AFM) Néel vector via spin-orbit torque. Measurements employing multiterminal patterned structures of Pt/AFM show recurring signals of the supposedly planar Hall effect and magnetoresistance, implying AFM switching. We show in this Letter that similar signals have been observed in structures with and *without* the AFM layer, and of an even larger magnitude using different metals and substrates. These may not be the conclusive evidence of spin-orbit torque switching of AFM, but the thermal artifacts of patterned metal structure on substrate. Large current densities in the metallic devices, beyond the Ohmic regime, can generate unintended anisotropic thermal gradients and voltages. AFM switching requires unequivocal detection of the AFM Néel vector before and after SOT switching.

DOI: [10.1103/PhysRevLett.123.227203](https://doi.org/10.1103/PhysRevLett.123.227203)

Purely electrical control of magnetic devices is an ultimate goal in spintronics. Previously, spin transfer torque (STT) could provide electrical switching of ferromagnetic (FM) layers but required at least two FM entities, e.g., Co/Cu/Co, where the spin-polarized current from one FM switches the magnetization of the other FM [1]. The recent discovery of spin-orbit torque (SOT) accommodates electrical switching of a single FM layer adjacent to a heavy metal (HM), such as in HM/FM bilayers [2–4]. Spin-orbit torque (SOT) switching is based on the spin Hall effect, where a charge current through the HM (e.g., Pt) with a large spin Hall angle θ_{SH} generates a pure spin current in the lateral direction with the spin index σ in the third direction. Above a threshold current density, the SOT can electrically switch the adjacent FM with in-plane anisotropy as well as perpendicular magnetic anisotropy, but the latter requires an external field along the current direction, and is thus highly undesirable. Several schemes have been demonstrated to achieve field-free SOT switching of the FM layer with perpendicular magnetic anisotropy [5–12].

It has been well established in both STT and SOT that switching of the magnetization \mathbf{M} of an FM layer occurs *only* when the current density j has exceeded the critical value j_c [1–12]. There is no appreciable change of \mathbf{M} at $j < j_c$, regardless of the duration of the current or the number of such current pulses. Only until $j \geq j_c$, swift and irreversible changes in \mathbf{M} occur. Switching (or lack thereof) can be readily revealed by the measurement of \mathbf{M} using magnetometry, or more simply, by suitable Hall effect and magnetoresistance (MR). The evidence for switching is unequivocal and can be readily verified by rotating \mathbf{M} of the FM via a small magnetic field to the specific directions.

The recent proposal of electrical switching via SOT of the antiferromagnetic (AFM) materials, with the potential of ushering in AFM spintronics with terahertz frequencies, has attracted much attention [13–18]. However, unlike FMs, AFMs have no net magnetization ($\mathbf{M} = 0$). They are weakly responsive to magnetic field, but display a rich variety of AFM spin structures from uniaxial to kagome lattice. Most theoretical and experimental studies of AFM switching have focused on the simplest AFMs with two colinear sublattice magnetizations in opposite directions $\mathbf{M}_1 = -\mathbf{M}_2$ defining a Néel vector $\mathbf{n}_{\text{Néel}} = (\mathbf{M}_1 - \mathbf{M}_2)/2M_0$, where M_0 is the magnitude of the sublattice magnetization. Theories suggest that the antidamping SOT, but not the fieldlike SOT, can switch the AFM Néel vector $\mathbf{n}_{\text{Néel}}$ with $\mathbf{M} = 0$ [19]. However, ascertaining electrical switching of the AFM Néel vector remains a formidable challenge, compounded by the fact that most AFMs have no well-defined $\mathbf{n}_{\text{Néel}}$.

Experimental exploration of AFM switching was first reported in epitaxial thin films of CuMnAs, an unusual metallic AFM with broken inversion symmetry [13]. As such, it is argued that CuMnAs (a similar situation also exists in Mn₂Au) affords Néel SOT switching without the necessity of an adjacent HM layer [13–15]. Most AFM switching studies have used Pt/NiO, where the SOT from Pt may switch NiO [16–18], a well-known AFM insulator. It has been assumed in the AFM switching studies that the AFM thin films would acquire the same AFM spin structures as those in bulk crystals, a premise that has not been borne out in extensive studies of exchange bias, which also involves AFM thin films [20].

To detect AFM switching, most studies have employed multiterminal structures, such as the four-terminal or the eight-terminal patterned structure. The eight-terminal

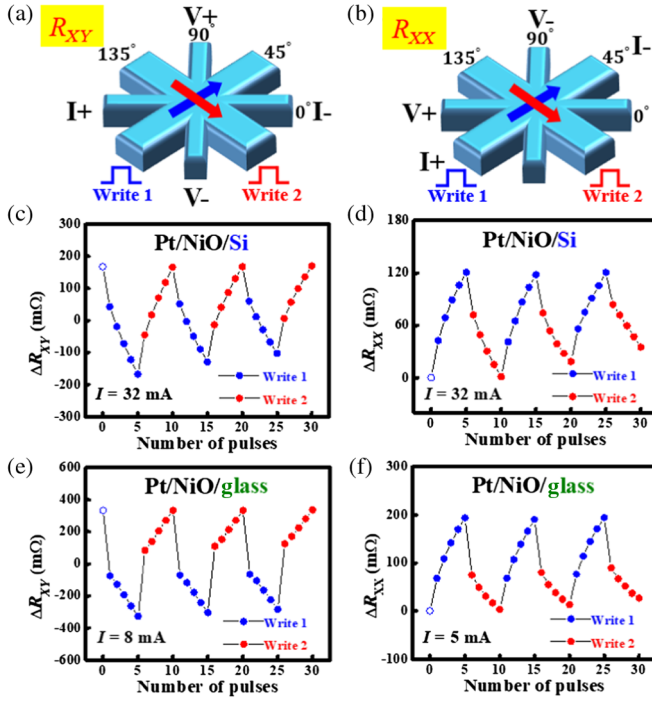


FIG. 1. Schematics of the eight-terminal patterned structure with the pulsed writing current along the 45° (write 1) and the 135° (write 2) lines for (a) planar Hall and (b) longitudinal resistance measurements. Relative changes of Hall resistance (ΔR_{XY}) in (c) Pt/NiO/Si and (e) Pt/NiO/glass and relative change of longitudinal resistance (ΔR_{XX}) in (d) Pt/NiO/Si and (f) Pt/NiO/glass, after applying 10-ms writing current pulses alternately along the 45° and the 135° lines.

structure, consisting of four electrical lines oriented at 0° , 45° , 90° , and 135° , is intended to capture the planar Hall effect (PHE) resistance R_{XY} in Fig. 1(a) and the MR resistance R_{XX} in Fig. 1(b) after the large writing current 1 (blue) and 2 (red) (along the 45° or 135° lines) switches the AFM Néel vector. The reading current and the measured voltage for both R_{XY} and R_{XX} are marked by $I+$, $I-$, $V+$, and $V-$ in Figs. 1(a) and 1(b). The MR may be the anisotropic MR in metallic AFMs [13–15] or the spin Hall MR in Pt/AFM bilayers [16–18,21–23]. We used the same patterned eight-terminal structure and obtained the same qualitative results as those in CuMnAS and Mn_2Au without HM, and in Pt/NiO. The crucial questions are whether or not these are evidence for SOT switching of the AFM Néel vector.

We use the *same* Pt(4)/NiO(60) bilayers, where polycrystalline 4 nm Pt and 60 nm NiO bilayers have been made by magnetron sputtering, onto substrate and patterned into the same eight-terminal devices with 20- μm wide writing leads along the 45° and the 135° directions, and 10- μm wide reading leads along the 0° and the 90° directions for R_{XY} and R_{XX} . For example, a writing current of 32 mA through the 20- μm wide Pt (4 nm) gives a current density of 4×10^7 A/cm². We use pulsed writing currents of magnitude I with the same pulse width of 10 ms. After a 10-s

delay time, the resistances R_{XY} and R_{XX} are subsequently measured at a much lower current density of 2.5×10^5 A/cm² from the reading leads. Our results of R_{XY} and R_{XX} of Pt(4)/NiO(60)/Si are shown in Figs. 1(c) and 1(d), respectively. They are expressed as the relative changes of Hall resistance ΔR_{XY} and longitudinal resistance ΔR_{XX} , where ΔR_{XY} steadily decreases (increases) with the number of writing current 1 blue (2 red) pulses of 32 mA along the 45° (135°) line, and ΔR_{XX} changes oppositely. The recurring results of ΔR_{XY} and ΔR_{XX} between write currents 1 and 2, very similar to those observed in CuMnAS, Pt/NiO, and Mn_2Au , have previously been claimed as evidence of SOT switching of AFMs [13–18]. However, these highly unusual results warrant closer analyses.

First of all, the results in Figs. 1(c) and 1(d) show that each current pulse of writing current 1 (blue) creates essentially the *same* incremental change in ΔR_{XY} and ΔR_{XX} . If these were related to AFM switching, it would imply that each current pulse would create a small but similar Néel vector rotation and/or AFM domain reversal. The extent of AFM switching would scale with the *number* of pulses, i.e., more pulses would cause a larger portion of switching. Reverting to writing current 2 (red), each current pulse would create the *same* but *reversed* incremental change in AFM switching. These behaviors, if indeed due to AFM switching, would be diametrically different from those known in SOT or STT switching of FM systems, where, at $j < j_c$, there are no incremental changes, nor reversed incremental changes, nor accumulative changes of magnetization reversal at all [1–12].

It is also important to stress the large writing current of 32 mA with a high current density of 4×10^7 A/cm² in Figs. 1(c) and 1(d). At $I < 25$ mA, we obtained only $R_{XY} \approx 0$ and $\Delta R_{XY} \approx 0$; $R_{XX} \approx \text{constant}$ and $\Delta R_{XX} \approx 0$. Only with a larger current, e.g., 32 mA, could we measure appreciable R_{XY} , ΔR_{XY} , and ΔR_{XX} , the size of which *scales* with the write current I . At a slightly higher current of $I \approx 35$ mA the sample was destroyed. We illustrate these aspects with another nominally the same Pt(4)/NiO(60)/Si sample from low current to the breakdown current using one-shot pulses, as shown in Fig. 2. Below 25 mA, $R_{XY} \approx 0$ and $\Delta R_{XY} \approx 0$; $R_{XX} \approx 90.6 \Omega$ and $\Delta R_{XX} \approx 0$, and these values are independent of I . This is the Ohmic regime, in which the voltage is linearly proportional to current yielding a constant resistance independent of current. The Ohmic regime is where resistance measurements of any metal are normally made, with a lower current to avoid excessive joule heating. The results of $R_{XY} \approx 0$ and $\Delta R_{XY} \approx 0$ indicate there is no PHE signal, i.e., no evidence of AFM switching.

However, at $I > 25$ mA, R_{XY} and R_{XX} rise sharply with I , as shown in Figs. 2(a) and 2(c), respectively, i.e., highly non-Ohmic, and at 42 mA the device breaks down. Only in the non-Ohmic regime with a very high current can one observe the sizable changes for ΔR_{XY} and ΔR_{XX} on pulse

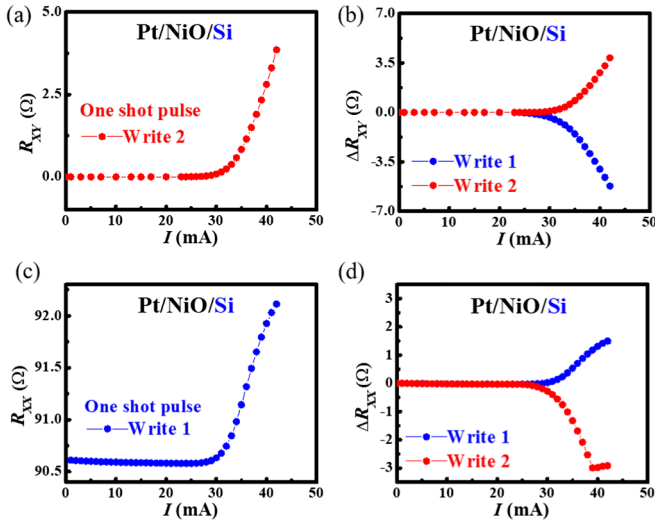


FIG. 2. (a) R_{XY} and (b) ΔR_{XY} in Pt/NiO/Si as a function of one-shot writing current pulses along the 45° (write 1) or the 135° (write 2) lines. (c) R_{XX} and (d) ΔR_{XX} in Pt/NiO/Si as a function of one-shot current pulse along the 45° (write 1) or the 135° (write 2) lines.

writing current with different orientations, as shown in Fig. 2(b). The values of R_{XX} , ΔR_{XX} , R_{XY} , and ΔR_{XY} are not constant but rise sharply with I . Thus, the evidence of AFM switching to date, the increasing and decreasing ΔR_{XY} , could just be the result of the resistance measurements in the non-Ohmic regime at very high current density, below the breakdown current. The high current density exceeding 10^7 A/cm² also develops serious thermal issues with irreversible damages due to intense heat and electromigration. After such high current densities, the resistance of the metallic device has suffered permanent changes.

Since R_{XY} and R_{XX} are electrical characteristics, one expects the results to be intrinsic to Pt(4)/NiO(60) and independent of the insulating substrate on which the patterned Pt(4)/NiO(60) structures are situated. Quite the contrary, we found both R_{XY} and R_{XX} depend greatly on substrates. The results of the same patterned structures on glass, as shown in Figs. 1(e) and 1(f), are much larger than those on Si, with those on MgO in between (not shown). This indicates a strong influence of substrate for electrical measurements at very high current density, in particular, the heat dissipation through the substrate. The larger ΔR_{XY} and ΔR_{XX} for structures on glass, as compared to those on Si, are due to the lower thermal conductivity κ of glass as shown in Table I. Therefore, the same structures when patterned on glass substrate exhibit similar signals but of far greater magnitude. Note that the writing current in Pt/NiO/glass [Fig. 1(e)] is only 8 mA, but the values of ΔR_{XY} are much larger than those for Pt/NiO/Si [Fig. 1(c)] at 32 mA. Likewise, the ΔR_{XX} for Pt/NiO/glass shown in Fig. 1(f) at 5 mA are much larger than those for Pt/NiO/Si at 32 mA shown in Fig. 1(d). Because of the much lower κ

TABLE I. Thermal conductivity of Si, MgO, and glass [24]. Simulation of rising temperature in Pt (4 nm) on Si, MgO, and glass and temperature difference between T_1 and T_2 in Fig. 4(a), after applying one-shot writing current of density of 1.75×10^7 A/cm².

Substrate	Thermal conductivity			
	(W/mK)	T_1 (K)	T_2 (K)	ΔT (K)
Silicon	131	301.25	301.36	0.11
MgO	30	304.92	305.38	0.46
Glass	1.38	383.64	393.78	10.14

for glass, Pt/NiO/glass also has a much lower onset current for the non-Ohmic regime and breakdown current than those for Pt/NiO/Si. Since only the writing current dictates the strength of the SOT that switches the Néel vector of the AFM NiO, the large variations in ΔR_{XX} , ΔR_{XY} , and the onset writing current due to different substrates strongly indicate these are not evidence of SOT switching of the AFM Néel vector.

We further patterned the same eight-terminal structure on Si, MgO, and glass with only the metal Pt and *without* the AFM layer of NiO, thus removing any possibility of AFM switching. Still, the *same* sawtooth recurring patterns in ΔR_{XY} and ΔR_{XX} can be observed, as shown in Fig. 3. These signals, without NiO, increase in the order of Pt/Si, Pt/MgO, and Pt/glass, reflecting the thermal conductivity of the substrates, and illustrating that these recurring results are non-Ohmic joule heating in Pt only. Thus, the recurring sawtooth signals in Pt/NiO are unrelated to SOT AFM switching.

The eight-terminal devices were designed to exploit the PHE and MR to reveal the SOT switching of the AFM Néel vector. While the PHE and MR are established methods for

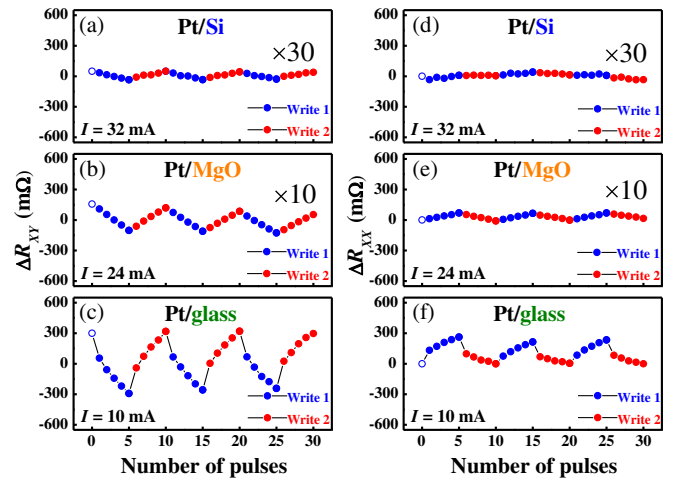


FIG. 3. The values of ΔR_{XY} and ΔR_{XX} after applying successive writing pulses current alternately along the 45° and the 135° lines for (a) Pt/Si, (b) Pt/MgO, and (c) Pt/glass; and for (d) Pt/Si, (e) Pt/MgO, and (f) Pt/glass, respectively, without any AFM.

detecting the direction of \mathbf{M} of the FM layer, they have never been demonstrated for detecting the Néel vector of an AFM layer, for there is no simple method to create and orient the AFM Néel vector to the specific directions on demand. Unfortunately, the eight-terminal patterned structure also creates unforeseen complications in electrical measurements. The eight terminals are connected to the same *common* area, which receives the writing current of a large current density and whose electrical characteristics are subsequently measured to assess possible AFM switching. The intended PHE and MR results inadvertently include unintended contributions of the asymmetrical temperature gradient, thermal voltages, and Hall voltages.

Only a high writing current beyond the Ohmic regime, with a current density in the 10^7 A/cm² range, generates measurable values of R_{XY} and ΔR_{XY} . After the application of a writing current 1 (blue) pulse, there is a large temperature rise in the 45° line, by more than 100 K, as corroborated by the COMSOL simulation as shown in Figs. 4(a) and 4(c), which creates a net temperature gradient between the voltage leads in the 90° line. For the R_{XY} measurements, the current and voltage leads are along the 0° and the 90° lines, respectively. This leads to the Seebeck effect in the direction of the temperature gradient. Any metal (e.g., Pt, Cr, and Au) with a significant Seebeck effect gives rise to a thermal voltage with an increasing magnitude

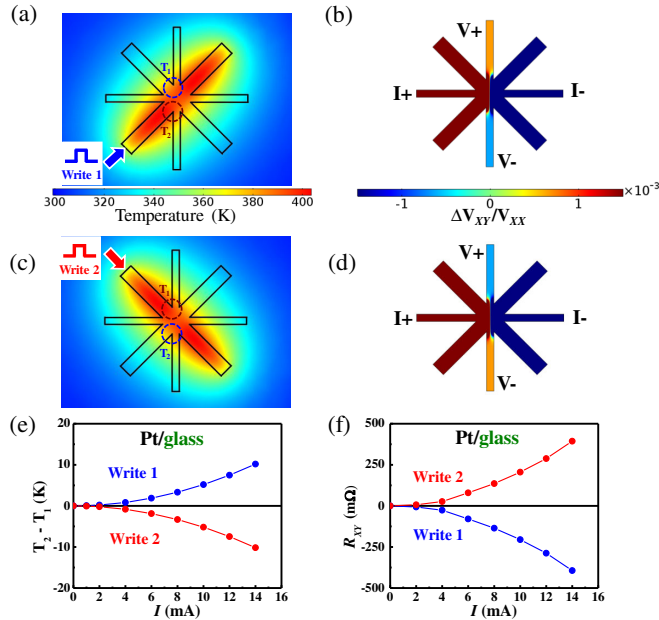


FIG. 4. Simulation of temperature distribution for the eight-terminal patterned Pt/glass structure after applying one-shot current of density 1.75×10^7 A/cm² along (a) 45° (write 1) and (c) 135° (write 2) lines. Simulation of Hall signal induced after one-shot writing current along (b) 45° (write 1) and (d) 135° (write 2) lines with the relative Seebeck coefficient of $8 \mu\text{V}/\text{K}$. (e) The temperature difference between T_1 and T_2 and (f) R_{XY} as a function of one-shot current pulse along 45° (write 1) and (c) 135° (write 2) lines.

for each successive writing current 1 (blue) pulse. When one reverts to the writing current 2 (red), the 135° line is heated. As compared with Figs. 4(b) and 4(d), the temperature gradient between the voltage leads in the 90° line now reverses to give an opposite sign of thermal voltage, that increases with each of the successive writing current pulses. The simulation values are qualitatively consistent with experiments with a relative Seebeck coefficient around $8 \mu\text{V}/\text{K}$ [25,26]. These temperature differences and voltages scale sharply with the current as shown in Figs. 4(e) and 4(f), giving the appearance of recurring Hall resistance signals, by the same token, the MR voltage as well, as shown in Supplemental Material Fig. S1 [27]. In addition to Pt, we have also patterned Cr and Au. As shown in Supplemental Material Fig. S2 [27], the signals for Cr are much larger than those of Pt and Au because of the larger Seebeck coefficient of Cr [29]. These thermal voltages, intrinsic to the metal layer of Pt, Au, and Cr, have nothing to do with AFM switching.

Previous studies of AFM switching have noted the intense heat in the device [30,31]. Some protocols, e.g., a pause of 10 s after the writing current pulse before the electrical measurements, have been used to alleviate the heating problem. Our measurements reveal that 10 s is far too short for the intense heat to dissipate. In fact, we have found a sizable ΔR_{XY} and temperature gradient remains in the patterned structures even after one hour. Very high current density may also anneal the thin films, cause electromigration and other irreversible damages, causing permanent changes of the resistance, as shown in Supplemental Material Fig. S2 [27]. Furthermore, after the sample has been subjected to a high writing current pulse, subsequent measurements at a lower current may reveal a sawtooth of different magnitudes, and in some cases, even altering the sawtooth shape into steplike signals [32], as illustrated in Supplemental Material Fig. S3 [27]. Recent experiments also indicate a non-spin-torque origin of AFM switching [33].

In summary, much attention has been focused recently on SOT switching of AFM Néel vector employing multi-terminal patterned structures that show recurring signals in PHE ΔR_{XY} and MR ΔR_{XX} signals. We show in this work that these voltage and resistance signals may not be conclusive evidence of SOT switching of AFM, but the artifacts of the large writing currents beyond the Ohmic regime through the metallic multiterminal devices. The prospect of SOT switching of AFM Néel vector encounters numerous challenges. Many AFMs have complex spin structures without a well-defined Néel vector. Even for AFMs that may accommodate a Néel vector, it remains a challenge to unequivocally detect the AFM Néel vector, before and after the SOT switching.

This work was supported by the Ministry of Science and Technology of Taiwan, under the Grant No. MOST 106-2628-M-002-015-MY3. This work was also partially

supported by Academia Sinica and National Taiwan University. We thank D. Y. Kang and C. T. Chen from National Taiwan University for simulation support. Work at JHU was supported by KAUST (Grant No. OSR2017-CRG6-3427.01) and the U.S. Department of Energy (Award No. DE-SC0009390 and No. SC0012670).

*syhuang@phys.ntu.edu.tw

- [1] E. B. Myers, D. C. Ralph, J. A. Katine, R. N. Louie, and R. A. Buhrman, *Science* **285**, 867 (1999); D. C. Ralph and M. D. Stiles, *J. Magn. Magn. Mater.* **320**, 1190 (2008).
- [2] L. Liu, C. F. Pai, Y. Li, H. W. Tseng, D. C. Ralph, and R. A. Buhrman, *Science* **336**, 555 (2012).
- [3] I. M. Miron, K. Garello, G. Gaudin, P. J. Zermatten, M. V. Costache, S. Auffret, S. Bandiera, B. Rodmacq, A. Schuhl, and P. Gambardella, *Nature (London)* **476**, 189 (2011).
- [4] L. Liu, O. J. Lee, T. J. Gudmundsen, D. C. Ralph, and R. A. Buhrman, *Phys. Rev. Lett.* **109**, 096602 (2012).
- [5] G. Yu, P. Upadhyaya, Y. Fan, J. G. Alzate, W. Jiang, K. L. Wong, S. Takei, S. A. Bender, L. T. Chang, Y. Jiang, M. Lang, J. Tang, Y. Wang, Y. Tserkovnyak, P. K. Amiri, and K. L. Wang, *Nat. Nanotechnol.* **9**, 548 (2014).
- [6] L. Youa, O. Leea, D. Bhowmika, D. Labanowskia, J. Honga, J. Bokora, and S. Salahuddin, *Proc. Natl. Acad. Sci. U.S.A.* **112**, 10310 (2015).
- [7] Y. W. Oh, S. H. Chris Baek, Y. M. Kim, H. Y. Lee, K. D. Lee, C. G. Yang, E. S. Park, K. S. Lee, K. W. Kim, G. Go, J. R. Jeong, B. C. Min, H. W. Lee, K. J. Lee, and B. G. Park, *Nat. Nanotechnol.* **11**, 878 (2016).
- [8] S. Fukami, C. Zhang, S. DuttaGupta, A. Kurenkov, and H. Ohno, *Nat. Mater.* **15**, 535 (2016).
- [9] A. van den Brink, G. Vermijs, A. Solignac, J. Koo, J. T. Kohlhepp, H. J. Swagten, and B. Koopmans, *Nat. Commun.* **7**, 10854 (2016).
- [10] Q. Ma, Y. Li, D. B. Gopman, Y. P. Kabanov, R. D. Shull, and C. L. Chien, *Phys. Rev. Lett.* **120**, 117703 (2018).
- [11] S. C. Baek, V. P. Amin, Y. W. Oh, G. Go, S. J. Lee, G. H. Lee, K. J. Kim, M. D. Stiles, B. G. Park, and K. J. Lee, *Nat. Mater.* **17**, 509 (2018).
- [12] T. C. Chuang, C. F. Pai, and S. Y. Huang, *Phys. Rev. Applied* **11**, 061005 (2019).
- [13] P. Wadley *et al.*, *Science* **351**, 587 (2016).
- [14] S. Yu. Bodnar, L. Šmejkal, I. Turek, T. Jungwirth, O. Gomonay, J. Sinova, A. A. Sapozhnik, H.-J. Elmers, M. Kläui, and M. Jourdan, *Nat. Commun.* **9**, 348 (2018).
- [15] X. F. Zhou, J. Zhang, F. Li, X. Z. Chen, G. Y. Shi, Y. Z. Tan, Y. D. Gu, M. S. Saleem, H. Q. Wu, F. Pan, and C. Song, *Phys. Rev. Applied* **9**, 054028 (2018).
- [16] X. Z. Chen, R. Zarzuela, J. Zhang, C. Song, X. F. Zhou, G. Y. Shi, F. Li, H. A. Zhou, W. J. Jiang, F. Pan, and Y. Tserkovnyak, *Phys. Rev. Lett.* **120**, 207204 (2018).
- [17] T. Moriyama, K. Oda, T. Ohkochi, M. Kimata, and T. Ono, *Sci. Rep.* **8**, 14167 (2018).
- [18] L. Baldrati, O. Gomonay, A. Ross, M. Filianina, R. Lebrun, R. Ramos, C. Leveille, T. Forrest, F. Maccherozzi, E. Saitoh, J. Sinova, and M. Kläui, [arXiv:1810.11326v1](https://arxiv.org/abs/1810.11326v1).
- [19] V. Baltz, A. Manchon, M. Tsoi, T. Moriyama, T. Ono, and Y. Tserkovnyak, *Rev. Mod. Phys.* **90**, 015005 (2018).
- [20] J. Nogué and I. K. Schuller, *J. Magn. Magn. Mater.* **192**, 203 (1999).
- [21] G. R. Hoogeboom, A. Aqeel, T. Kuschel, T. T. M. Palstra, and B. J. van Wees, *Appl. Phys. Lett.* **111**, 052409 (2017).
- [22] J. Fischer, O. Gomonay, R. Schlitz, K. Ganzhorn, N. Vlietstra, M. Althammer, H. Huebl, M. Opel, R. Gross, S. T. B. Goennenwein, and S. Geprägs, *Phys. Rev. B* **97**, 014417 (2018).
- [23] L. Baldrati, A. Ross, T. Niizeki, C. Schneider, R. Ramos, J. Cramer, O. Gomonay, M. Filianina, T. Savchenko, D. Heinze, A. Kleibert, E. Saitoh, J. Sinova, and M. Kläui, *Phys. Rev. B* **98**, 024422 (2018).
- [24] S. Y. Huang, D. Qu, and C. L. Chien, *Charge, Solid State Physics* (Academic Press, Oxford, 2013), Vol. 64, pp. 53–82.
- [25] Y.-J. Chen and S.-Y. Huang, *Phys. Rev. Lett.* **117**, 247201 (2016).
- [26] T. C. Chuang, P. L. Su, P. H. Wu, and S. Y. Huang, *Phys. Rev. B* **96**, 174406 (2017).
- [27] See Supplemental Material at <http://link.aps.org/supplemental/10.1103/PhysRevLett.123.227203> for more details on COMSOL simulations for eight and four terminal devices, the time dependent Hall resistance with different substrates and normal metals, and the evolution between the sawtooth and the steplike switching behaviors, which includes Ref. [27].
- [28] G. A. Slack, *J. Appl. Phys.* **35**, 339 (1964).
- [29] W. M. Haynes, *CRC Handbook of Chemistry and Physics* (CRC Press, Oakville, 2014), 95th ed.
- [30] M. Meinert, D. Graulich, and T. Matalla-Wagner, *Phys. Rev. Applied* **9**, 064040 (2018).
- [31] T. Matalla-Wagner, M.-F. Rath, D. Graulich, J.-M. Schmalhorst, G. Reiss, and M. Meinert, [arXiv:1903.12387](https://arxiv.org/abs/1903.12387).
- [32] Y. Cheng, S. Yu, M. Zhu, J. Hwang, and F. Yang, [arXiv:1906.04694](https://arxiv.org/abs/1906.04694).
- [33] P. Zhang, J. Finley, T. Safi, J. Han, and L. Liu, [arXiv:1907.00314](https://arxiv.org/abs/1907.00314).